CERN-TH-2019-088

Dynamical Friction in Interacting Relativistic Systems

Andrey Katz,[1,2] Aleksi Kurkela,[1,3] and Alexander Soloviev[4]

[1] *TH Department, CERN, 1 Esplanade des Particules, 1211 Geneva 23, Switzerland*

[2] *Université de Genève, Department of Theoretical Physics and Center for Astroparticle Physics (CAP), 24 quai E. Ansermet, CH-1211, Geneva 4, Switzerland*

[3] *Faculty of Science and Technology, University of Stavanger, 4036 Stavanger, Norway*

[4] *Institut für Theoretische Physik, Technische Universität Wien, Wiedner Hauptstr. 8-10, A-1040 Vienna, Austria*

(Dated: June 14, 2019)

We study dynamical friction in interacting relativistic systems with arbitrary mean free paths and medium constituent masses. Our novel framework recovers the known limits of ideal gas and ideal fluid when the mean free path goes to infinity or zero, respectively, and allows for a smooth interpolation between these limits. We find that in an infinite system the drag force can be expressed as a sum of ideal-gas-like and ideal-fluid-like contributions leading to a finite friction even at subsonic velocities. This simple picture receives corrections in any finite system and the corrections become especially significant for a projectile moving at a velocity v close to the speed of sound $v \approx c_s$. These corrections smoothen the ideal fluid discontinuity around the speed of sound and render the drag force a continuous function of velocity. We show that these corrections can be computed to a good approximation within effective theory of viscous fluid dynamics.

arXiv:1906.05341v1 [hep-ph] 12 Jun 2019

I. INTRODUCTION

Dynamical friction—or how a projectile that moves through a medium is slowed down by the gravitational interaction with the medium—is a classic problem that has many applications, primarily in astrophysics. It was first addressed by Chandrasekhar [1], who considered the gravitational force exerted on a projectile that moves non-relativistically through a gas of heavy, non-interacting particles. The primary motivation of Chandrasekhar's work was to understand the drag force exerted on a star in a "gas" of other stars. However, there are many modern questions in astro-particle and beyond-the-standard-model physics involving the gravitational interaction of a projectile with its surrounding medium—such as, *e.g.*, the propagation of primordial black holes or other dark-matter candidates through neutron stars [2–5]—which cannot be reduced to non-relativistic movement in a dilute gas, motivating further analysis of dynamical friction in more general systems.

Chandrasekhar's result has indeed been generalized to many different systems. For example, the first analysis of the relativistic projectile propagating through a non-interacting gas of photons was performed in [6]. However, the interpolation between these two limits of non-relativistic and ultra-relativistic media has so far remained unknown. Besides mere kinematics, dynamical friction depends crucially also on the self-interaction of the medium constituents. If the interaction between the medium constituents is strong enough, it is more appropriate to describe the medium as an ideal fluid rather than as an ideal gas—a case studied in [7–11]. Again, how one interpolates between the two limits of ideal gas and ideal fluid in a system with finite mean free path remains an open question.

In this work we develop a simple diagrammatic field-theory formalism to evaluate dynamical friction in a wide class of relativistic interacting systems with a finite mean free path, $l_{\rm mfp}$. Dynamical friction arises from the projectile moving up the gravitational potential it itself created by gravitationally perturbing the medium through which it propagates. The shape of the wake—and hence its gravitational field—depends on the material properties of the medium that in an interacting system depend on the length scale considered. At short length scales $\Delta x \ll l_{\rm mfp}$, the medium appears as an ideal gas and corrections may be computed in powers of $\Delta x/l_{\rm mfp}$. In the opposite limit of long length scales $\Delta x \gg l_{\rm mfp}$, the interacting medium behaves as an ideal fluid, a picture that can be systematically improved by taking into account higher-order "viscous" corrections appearing in powers of $l_{\rm mfp}/\Delta x$ in fluid-dynamic gradient expansion [12].

Due to the long-distance nature of the gravitational force, all length scales contribute equally to dynamical friction. In an interacting medium where the mean free path fits inside the medium $R_{\rm max} > l_{\rm mfp}$ but is larger than the size of the projectile $R_{\rm min} < l_{\rm mfp}$, the drag force receives both ideal-gas- and ideal-fluid-like contributions

$$F = c_{\rm gas} \log\left(\frac{R_{\rm min}}{l_{\rm mfp}}\right) + c_X + c_{\rm fluid} \log\left(\frac{l_{\rm mfp}}{R_{\rm max}}\right), \tag{1}$$

where the logarithmically enhanced terms arise from all scales much shorter ($c_{\rm gas}$) or much longer ($c_{\rm fluid}$) than the mean free path. These logarithmically enhanced terms are universal in the sense that they depend only on few characteristics of the medium: the ideal-fluid-like contribution depends only on the speed of sound, whereas the ideal-gas-like contribution depends on an integral moment of the velocity distribution. All the information about the interactions can be encapsulated in a single subleading-log contribution c_X.

We compute the drag force using a field-theory approach in which the force—to leading order in Newton's constant—is given by the in-medium-dressed graviton propagator (see Fig. 1). The

computation therefore boils down to finding the graviton polarization tensor that dresses the tree-level graviton propagator. The polarization tensor that is given by the Green function of the energy-momentum tensor characterizes the medium and is known in variety of media. Here, we consider freely streaming gas, viscous fluid dynamics, and interacting kinetic theory in relaxation-time approximation [12, 13].

In the limit of ideal fluid dynamics, the drag force vanishes exactly for subsonic projectiles and the force has a discontinuity when crossing the sound barrier $v = c_s$ [7]. We find that in the fluid-dynamic limit, dynamical friction can be understood as emission of real "on-shell" phonons forming a Mach cone transporting energy far away from the projectile. This explains in an intuitive way the lack of dynamical friction for a subsonic projectile that has phase-space to excite only "virtual" phonons which do not propagate far. We further find that dissipative, viscous effects are always large for projectile velocities near the speed of sound $v \approx c_s$. For these velocities a description of the medium in terms of ideal fluid is never applicable and viscous effects always lead to $\mathcal{O}(1)$ corrections. These corrections smoothen the discontinuity of the drag force in any system with a finite interaction rate (for other effects removing the discontinuity, see [10, 14]). By computing these subleading-log contributions in interacting kinetic theory and in viscous fluid dynamics we find that they can be well approximated by the latter.

We note that also our treatment makes two assumptions to simplify the problem. First, we will restrict ourselves to a regime, where the accretion onto the projectile that propagates through the medium is negligible. This is always the case if the radius of the bullet is much bigger than the accretion radius, however, this condition can also be satisfied in a broader framework. Clearly this is not always the case,*e.g.*, if the projectile is a non-relativistic black hole. However, it has been previously shown in explicit numerical simulations that even if the accretion effects are maximized, they never dominate over dynamical friction [15]. Second, we restrict ourselves to the regime of linearized gravity. We will briefly explain, however, how our formalism can potentially be used to capture the post-Newtonian corrections.[1]

Our paper is structured as follows. In Sec II we present our formalism in detail and explain the logic behind the calculation. The calculation itself is performed in Sec III. We begin by analyzing the fluid-dynamical case, starting from the well-known inviscid fluid and then continuing to the more complicated scenario with non-vanishing viscosity. We then move on to the ideal-gas regime, reproducing the well-known results of the non-relativistic and ultra-relativistic approximations. Finally we perform the full calculation for the interacting gas in relaxation time approximation

[1] For earlier works that address the post-Newtonian corrections to the dynamical friction see [15, 16].

that interpolates between all of these cases. The boundary effects are very briefly addressed in Sec IV. In the last section we draw our conclusions and discuss the application of our results for real-words problems.

II. DESCRIPTION OF THE FORMALISM

Our main objective is to calculate the drag force, exerted on gravitating point source—or the *bullet* from here onwards—that propagates through yet-to-be-specified static and infinite medium. In the linearized regime, the four-force F^μ exerted on the bullet of mass m_b by the gravitational field of its own wake h^{wake} can be written as

$$F^\mu = \frac{\mathrm{d}p^\mu}{\mathrm{d}t} = -\frac{m}{\gamma}\Gamma^\mu{}_{\alpha\beta}(h^{wake})u^\alpha u^\beta, \tag{2}$$

where $u^\mu = \gamma(1, \vec{v})$ is the four-velocity of the bullet. The zero component corresponds to the rate of energy loss $F^0 = \frac{\mathrm{d}E}{\mathrm{d}t}$. If the projectile in question has dimensions comparable to its Schwarzschild radius, this approximation breaks down at short distances where non-linear effects in gravity start to play a non-negligible role. However, this is expected to happen at distances strictly smaller than the accretion radius [15] where our calculation is insufficient anyways. Therefore we shall adopt this approximation through out the paper.

A. The wake

We start by deriving a formal expression of the gravitational field of the bullet's wake in a form that makes minimal assumptions about the structure of the medium. We assume that before the medium is perturbed by the projectile, the medium is homogeneous and isotropic such that its unperturbed energy-momentum tensor reads[2]

$$T^{medium}_{\mu\nu} = \begin{pmatrix} \rho & 0 & 0 & 0 \\ 0 & P & 0 & 0 \\ 0 & 0 & P & 0 \\ 0 & 0 & 0 & P \end{pmatrix} \tag{3}$$

with energy density ρ and pressure P. We assume that the unperturbed background metric can be treated as locally flat $g^{(0)}_{\mu\nu} = \eta_{\mu\nu}$. Note however that for strongly self-gravitating objects this locally flat frame can be significantly different from the observer's frame.

[2] Our metric in this paper is "mostly plus", namely $(-+++)$.

For large separations, the projectile affects the medium by inducing a linear perturbation of the gravitational field

$$g_{\mu\nu} = \eta_{\mu\nu} + h^{bullet}_{\mu\nu}. \tag{4}$$

The gravitational perturbation $h^{bullet}_{\mu\nu}$ caused by the bullet is conveniently found by convoluting the energy-momentum tensor of the bullet with the Green function of the linearized Einstein equation, *i.e.*, with the graviton propagator[3]

$$h^{bullet}_{\mu\nu}(x) = \int d^4x' G^{grav}_{\mu\nu,\alpha\beta}(x,x') T^{\alpha\beta}_{bullet}(x'). \tag{5}$$

Assuming that the bullet of mass m_b moves with a constant velocity v through the medium in z-direction, the energy momentum tensor of the bullet and its Fourier transform can be written as[4]

$$T^{\mu\nu}_{bullet}(t,\vec{x}) = \frac{m_b}{\gamma} u^\mu u^\nu \delta(z-vt)\delta^2(x_\perp), \tag{6}$$

$$\tilde{T}^{\mu\nu}_{bullet}(\omega,\vec{k}) = \frac{2\pi m_b}{\gamma} u^\mu u^\nu \delta(\omega - k^z v), \tag{7}$$

where $u^\mu = \gamma(1,0,0,v)$ is the four-velocity vector of the bullet.

The linear perturbation in the gravitational field caused by the bullet will in turn cause a linear perturbation in the background medium. How this perturbation evolves in time depends on the material properties of the medium. For now, we will not specify the properties of the medium. However, in general, the medium response of the energy-momentum tensor $\delta T^{\mu\nu}$, can be characterized by its retarded Green function G_{medium}

$$\delta T^{\mu\nu}_{wake}(x) = \int d^4x' G^{\mu\nu,\alpha\beta}_{medium}(x',x) h^{bullet}_{\alpha\beta}(x'). \tag{8}$$

The response function depends on the microscopic dynamical properties of the medium and Eq. (8) needs to be eventually supplemented with an appropriate Green function characterizing the medium. The Green function is known is some special cases, *e.g.*, in free-streaming gas and in ideal liquid (or even in some quantum field theories [17]); we reproduce these limits in the appendices and extend the calculation of the Green function to massive interactive kinetic theory.

Finally, the wake itself will have its own gravitational field, which can again be computed using the Green function of the linearized Einstein equation

$$h^{wake}_{\mu\nu}(x) = \int d^4x' G^{grav}_{\mu\nu,\alpha\beta}(x,x') T^{\alpha\beta}_{wake}(x'). \tag{9}$$

---

[3] Here, we work in the harmonic (de Donder) gauge, see appendix A for details.

[4] We work with the convention $f(x) = \int \frac{d^4k}{(2\pi)^4} e^{ik\cdot x} f(k)$. Further, we will be interested in retarded Green functions, and therefore to pick the retarded ordering, we must take $\omega \equiv k^0$ to have a small positive imaginary part $\omega + i\epsilon$.

That is, h^{wake} represents the gravitational field that was created by a wake that was created by a gravitational field that was created by the bullet. In Fourier space, where the convolution becomes a simple product of the Green functions, the gravitational field of the wake has a particularly simple form

$$h^{wake}_{\mu\nu}(\omega,\vec{k}) = G^{dressed}_{\mu\nu,\alpha\beta}(\omega,\vec{k})T^{\alpha\beta}_{bullet}(\omega,\vec{k}) \tag{10}$$

in terms of the retarded in-medium dressed graviton propagator

$$G^{dressed}_{\mu\nu,\alpha\beta}(\omega,\vec{k}) = G^{grav}_{\mu\nu,\gamma\delta}(\omega,\vec{k})G^{\gamma\delta,\rho\sigma}_{medium}(\omega,\vec{k})G^{grav}_{\rho\sigma,\alpha\beta}(\omega,\vec{k}). \tag{11}$$

B. The force

Once we know the expression for the gravitational field of the wake, the force that is exerted on the bullet becomes straightforward to calculate. Manifestly, Eq. (2) reads in components

$$F^z = -m\gamma(\Gamma^z{}_{00} + 2v\Gamma^z{}_{0z} + v^2\Gamma^z{}_{zz}) = -m\gamma\left(-\frac{1}{2}\partial_z h^{wake}_{00} + \partial_0 h^{wake}_{0z} + (v\partial_0 + v^2\frac{1}{2}\partial_z)h^{wake}_{zz}\right), \tag{12}$$

where the above expression is evaluated along the worldline of the bullet $z = vt$. The expression has a particularly simple interpretation in the non-relativistic limit, where only the first term contributes and h_{00} can be identified as the Newtonian gravitational potential: if the gravitational potential has a gradient along the direction of the movement of the bullet, the bullet does work climbing up the potential leading to energy loss.

The gradients of the different components of the gravitational-field perturbation are computed by inserting the energy-momentum tensor (7) to Eq. (10) and performing the inverse Fourier transform

$$\partial_\rho h^{wake}_{\mu\nu}(x) = i\frac{m_b u^\alpha u^\beta}{\gamma}\int \frac{d^4k}{(2\pi)^4}e^{ik\cdot x}k_\rho G^{dressed}_{\mu\nu,\alpha\beta}(k)2\pi\delta(\omega - k_z v), \tag{13}$$

which has a simple form along the worldline of the bullet

$$\partial_\rho h^{wake}_{\mu\nu}(z=vt) = i\frac{m_b u^\alpha u^\beta}{\gamma}\int \frac{\mathrm{d}^2k_\perp}{(2\pi)^2}\frac{\mathrm{d}k_z}{2\pi}k_\rho G^{dressed}_{\mu\nu,\alpha\beta}(\omega = vk_z + i\epsilon,\vec{k})\ . \tag{14}$$

The $+i\epsilon$ prescription chooses the appropriate boundary condition for the retarded propagator.

From Eq. (12) it is clear that the only relevant cases for our calculation are either $\rho = 0$ or $\rho = z$. In both of these cases the integral over dk_z in Eq. (14) can be further simplified by dividing the right-hand side into two equal parts and changing the integration variable $k_z \to -k_z$ in the latter

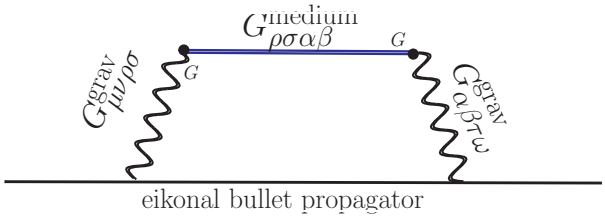

FIG. 1. Diagrammatic presentation of the calculation of the drag force of (16). It should be understood as a mixing of the linearized graviton with the excitation of medium. In the limiting cases of the hydrodynamics and the free streaming processes, these excitations becomes the sound and shear modes or the particle excitations, respectively.

part. As long as the background over which $G^{dressed}$ is computed is (time) translation invariant—as it is in all the cases we are considering—changing the sign of the real part of the frequency turns a retarded Green function into an advanced one, which is given by the complex conjugate of the retarded function. In all the cases that we are interested in, the retarded function is multiplied by a single power of k_z, such that we get

$$\int \frac{\mathrm{d}k_z}{2\pi} i k_z G^{dressed}_{\mu\nu,\alpha\beta} = \int \frac{\mathrm{d}k_z}{2\pi} \frac{ik_z}{2} (G^{dressed}_{\mu\nu,\alpha\beta} - (G^{dressed}_{\mu\nu,\alpha\beta})^*) = -\mathrm{Im} \int \frac{\mathrm{d}k_z}{2\pi} k_z G^{dressed}_{\mu\nu,\alpha\beta}. \tag{15}$$

With a little bit of algebra one can show that the force is then given simply by

$$F^z = -\frac{m^2_{\rm bullet}}{2\gamma^2} \mathrm{Im} \left[\int \frac{\mathrm{d}^2 k_\perp}{(2\pi)^2} \frac{\mathrm{d}k_z}{2\pi} k_z G^{dressed} \right], \tag{16}$$

with

$$G^{dressed} \equiv \left[G^{dressed}_{\mu\nu,\alpha\beta} \right] u^\mu u^\nu u^\alpha u^\beta, \tag{17}$$

where we additionally used that $(-v\omega + v^2 \frac{1}{2} k_z) = -\frac{v^2}{2} k_z$ and the explicit structure of the vector u^μ as it appears below Eq (7).

This expression has a simple diagrammatical representation, shown in Fig. 1. The dressed graviton propagator of (11) is connected to the *eikonal* propagator of the bullet (7) which forces the frequency $\omega = v k_z$.

C. Scale Separation and the Structure of the Drag Force

In the previous section we developed the machinery to calculate the drag force when the Green function of the energy-momentum tensor in medium is known. We now move on to discuss the generic properties of the Green functions and their implications to the structure of the drag force.

Irrespective of the microscopic details, any interacting matter with a finite mean free path $l_{\rm mfp}$ admits an effective late-time ($\Delta t \gg \tau_{\rm scat}$), long-distance ($\Delta x \gg l_{\rm mfp}$) description of the energy-momentum tensor in terms of relativistic fluid dynamics [12]. Relativistic fluid dynamics is based on a gradient expansion of the energy-momentum tensor around its equilibrium value

$$T_{\mu\nu} = T^{\rm eq}_{\mu\nu} + \Pi_{\mu\nu}, \tag{18}$$

$$T^{\rm eq}_{\mu\nu} = (\rho + P) u^{\rm fluid}_{\mu} u^{\rm fluid}_{\nu} + P g_{\mu\nu}, \tag{19}$$

where $u^{\rm fluid}_{\mu}$ is the rest frame of the fluid and the viscous shear-stress tensor, $\Pi_{\mu\nu}$, contains all possible terms consistent with symmetries constructed from the macroscopic quantities P, ρ, and $u_{\rm fluid}$ up to a given order in gradients. For ideal fluid dynamics the shear-stress tensor vanishes $\Pi_{\mu\nu} = 0$, whereas in first order viscous fluid dynamics the viscous shear-stress tensor is given by

$$\begin{aligned} \Pi_{\mu\nu} &= -2\eta\sigma_{\mu\nu} - \zeta \nabla_\alpha u^\alpha_{\rm fluid} \Delta_{\mu\nu}, \\ \sigma^{\alpha\beta} &= \frac{1}{2}\Delta^{\mu\alpha}\Delta^{\nu\beta}\Big(\nabla_\mu u^{\rm fluid}_\nu + \nabla_\nu u^{\rm fluid}_\mu - \frac{2}{3}\nabla_\alpha u^\alpha_{\rm fluid} g_{\mu\nu}\Big). \end{aligned} \tag{20}$$

where the shear η and bulk viscosities ζ are low-energy constants that describe the dissipative properties of the medium, and the projector on the subspace orthogonal to the flow velocity is given by $\Delta^{\mu\nu} \equiv u^\mu u^\nu + g^{\mu\nu}$. The higher-order corrections to ideal fluid dynamics are suppressed by powers of $l_{\rm mfp}/\Delta x \sim k l_{\rm mfp}$.

A simple dimensional analysis shows that the force in the ideal-fluid regime must be logarithmically divergent. The force in (16) must be parametrically

$$F^z \sim m^2_{\rm bullet} G^2 \int \frac{d^4k}{k^4} \times (\rho + P), \tag{21}$$

where the G^2/k^4 arises from the graviton propagator and is a reflection of the long-distance nature of the gravitational Coulomb potential. In absence of other available scales, the ideal fluid-dynamic energy-momentum tensor must be $\mathcal{O}(\rho+P)$ (see Appendix C for explicit expressions). As is evident from (21), all distance scales, $1/k$, contribute equally to the force. This leads to a logarithmic divergence when integral over all scales dk it taken. At large distance scales (corresponding to small wave numbers k), the divergence is regulated by dimensions of the medium $R_{\rm max}$. At small distance scales (large k), the divergences is regulated either by size of the bullet or by its accretion radius (whichever is bigger), $R_{\rm min}$, if the bullet is larger in size than the mean free path $l_{\rm mfp}$.

The higher-order corrections to the ideal fluid dynamics arise from terms with increasing number of gradients leading to corrections that become larger as k increases

$$F^z \sim m^2_{\rm bullet} G^2 \int \frac{d^4k}{k^4} \times (\rho + P) \left(1 + \mathcal{O}(l_{\rm mfp} k) + \mathcal{O}\left((l_{\rm mfp} k)^2\right) + \ldots\right). \tag{22}$$

The viscous corrections have stronger short-distance divergences (but are convergent at large distances), and they become increasingly more sensitive to the short-distance cutoff. If the short-distance cut-off is larger than the mean free path $R_{\rm min} > l_{\rm mfp}$, corrections to ideal fluid dynamics can be computed in hydrodynamical approximation to desired accuracy: in Sec III A 1 we provide the first viscous correction. However, if the intrinsic scale of the bullet is smaller than the mean free path $R_{\rm min} < l_{\rm mfp}$, the gradient expansion breaks down at scale $k \sim 1/l_{\rm mfp}$.

At scales shorter than the mean free path $k > 1/l_{\rm mfp}$ the matter behaves approximately as free-streaming. Also in the ideal gas, the drag force acquires equal contributions from all scales leading to logarithmic divergence. Now the interaction corrections come with increasing powers of $1/kl_{\rm mfp}$ (see *e.g.* [18]). Now the higher order terms are convergent at short distances but have increasingly strong long-distance divergences. That is, if the extent of the system is smaller than the mean free path $R_{\rm min} < l_{\rm mfp}$, the force can be computed in perturbative series of scattering corrections.

In systems where the mean free path fits inside the dimensions of the system the force gets contributions from all scales, the energy-momentum tensor can be approximated by fluid dynamics in the large-wave-length region and by free-streaming in the short-density region, which both lead to logarithmic divergences which are regulated by the dimension of the system and by the breakdown scale of the respective approximations

$$F^z = c_{\rm gas} \log\left(\frac{R_{\rm min}}{l_{\rm mfp}}\right) + c_X + c_{\rm fluid} \log\left(\frac{l_{\rm mfp}}{R_{\rm max}}\right) \ . \tag{23}$$

The logarithmically enhanced coefficients $c_{\rm fluid}$ and $c_{\rm gas}$ can be computed in ideal fluid dynamics and in free streaming systems, respectively. The contribution arising from scale $k \sim 1/l_{\rm mfp}$ gives rise to a subleading-log contribution, c_X, with no small expansion parameters.

This cross-over regime needs to be calculated in the full interacting kinetic theory, and it is sensitive to the microscopic details of the interactions. In a system with large scale separation between the geometric dimensions of the system and the mean free path, the ideal fluid and free-streaming contributions are logarithmically enhanced compared to the cross-over region arising from a single scale. However, as we will see in Section III A 2, this picture breaks down for $v \approx c_s$, irrespective of the value of $l_{\rm mfp}$.

III. CALCULATION OF THE DRAG FORCE

We now apply the formalism that we developed in the previous section to compute the dynamical friction in different regimes. We first start with a calculation in the fluid-dynamic regime. While

the ideal-fluid case is extensively covered in literature, we provide the first results for the viscous fluid. We then discuss the free streaming limit and extend the existing results by going beyond non-relativistic and ultra-relativistic approximations. Finally, we compute the drag force in a simple kinetic theory model that behaves as a free-streaming gas at short distance scales but exhibits fluid-dynamical behavior at large distance scales.

A. Fluid-dynamic limit

The form of retarded fluid-dynamic energy-momentum correlation function is well known; we briefly show this derivation in Appendix C. Using these results we can straightforwardly write the dressed (scalar mode) graviton propagator

$$G^{dressed}(\omega = vk^z) = \left(\frac{8\pi G\gamma^2}{-(\omega+i\epsilon)^2+\vec{k}^2}\right)^2 \left.\frac{f^{\rm ideal}_{\rm sound}(\omega,\vec{k})}{-(\omega+i\epsilon)^2+c_s^2k^2}\right|_{\omega=vk^z} \tag{24}$$

$$= \left(\frac{8\pi G\gamma^2}{(1-v^2)k_z^2+\vec{k}_\perp^2}\right)^2 \frac{f^{\rm ideal}_{\rm sound}(\vec{k}),}{(c_s^2-v^2)k_z^2+c_s^2\vec{k}_\perp^2-i\epsilon vk_z}. \tag{25}$$

The squared expression arises from the two graviton propagators. In ideal fluid dynamics, the perturbations of the energy-momentum tensor propagate by forming long-lived longitudinal density perturbations, *i.e.*, sound. The second propagator is a phonon—or sound-mode—propagator, characterized by the speed of sound $c_s^2 = dP/d\rho$. The numerator $f^{\rm ideal}_{\rm sound}$ reflects the coupling between gravity and sound modes and comes from the contractions of (11) and (17) with the sound-mode propagator of (C7)

$$f^{\rm ideal}_{\rm sound} = \frac{\rho+P}{2}\left[\frac{16k_z^2v^2\omega^2}{k^2} + \Big(\omega(8k_zv+(v^2-3)\omega) - k^2(v^2+1)\Big(c_s^2(v^2-3)-v^2-1\Big)\Big)\right] \tag{26}$$

As per (16), the drag force arises from the imaginary part of the above expression. As both the graviton and sound modes are long-lived, the above expression is real up to the $i\epsilon$ description. Then, an imaginary contribution can arise only when the the propagators go on shell, corresponding to a production of a long-lived mode. Because $(1-v^2) > 0$, the graviton propagators will never go on shell and the propagator is an analytic function of k^z for all v along the real k^z-axis. The same is true for the sound mode as long as $v < c_s$, and for subsonic velocities the propagator is perfectly analytic and the bullet feels no drag force in the inviscid fluid, in full agreement with [7]. That is, the gravitational field of the bullet excites only off-shell excitations in the fluid—virtual phonons— that cannot propagate far and make up the wake trailing the bullet. There is no phase space available to excite a real on-shell phonons that could carry energy asymptotically far away

from the bullet, and as energy cannot be given to long lived modes, there can be no total energy loss on the bullet because of energy conservation.

However, when the bullet moves with a supersonic velocity, namely $v^2 - c_s^2 > 0$, the phase space opens up for the sound mode propagator to go on shell when

$$k^z = k^z_{sound} = \pm \frac{c_s k_\perp}{\sqrt{v^2 - c_s^2}}, \tag{27}$$

leading to an imaginary part arising from the $i\epsilon$ prescription

$$\frac{1}{(c_s^2 - v^2)k_z^2 + c_s^2 \vec{k}_\perp^2 - i\epsilon v k_z} = \mathcal{P}\left(\frac{1}{(c_s^2 - v^2)k_z^2 + c_s^2 \vec{k}_\perp^2)}\right) + i\pi\delta\left((c_s^2 - v^2)k_z^2 + c_s^2 \vec{k}_\perp^2\right), \tag{28}$$

where $\mathcal{P}$ denotes the real principal value integral. Inserting (28) to (25) and further to (16) we get a simple form for the drag force

$$\frac{dF^z}{d\log k_\perp} = -\theta(v - c_s) m_b^2 4\pi G\gamma^2 \frac{(1+v^2)^2(P+\rho)}{v^2} \tag{29}$$

in agreement with [11].

That is, we see that the energy loss arises from transferring energy from the bullet to the long-lived asymptotic states—which in the case of fluid dynamics are the sound modes—that can transport the energy far away from the bullet. The condition (27) equivalently reads

$$\cos\theta = k_z/|k| = c_s/v \tag{30}$$

which is the angle in which the phonons are created and the unidirectional production of the sound waves is nothing but the sonic boom created by the bullet with the opening angle θ.

1. Viscous fluid

We are now ready to analyze a more realistic situation of the drag force in a viscous fluid. As we will immediately see, the drag force in a viscous fluid does not vanish in the subsonic regime.

In a viscous fluid, the gravitational field excites both sound (C7) and shear modes (C8) (but not the tensor mode (C9)) and using the fluid-dynamical Green function from Appendix C, the dressed propagator reads after straightforward calculation

$$G^{dressed} = \left(\frac{8\pi G\gamma^2}{-(\omega + i\epsilon)^2 + \vec{k}^2}\right)^2 \frac{f_{\rm sound}(\omega, \vec{k})}{-\omega^2 + c_s^2 k^2 - ik^2\Gamma_s\omega}\Big|_{\omega = vk^z} + \left(\frac{8\pi G\gamma^2}{-(\omega + i\epsilon)^2 + \vec{k}^2}\right)^2 \frac{f_{\rm shear}(\omega, \vec{k})}{\omega + i\eta_s k^2}\Big|_{\omega = vk^z} \tag{31}$$

In a viscous fluid, the sound modes are attenuated by diffusion and as a consequence the pole of the phonon propagator moves into the negative complex plane; $\Gamma_s k^2$ is the sound attenuation length

with $\Gamma_s = (\frac{4}{3}\eta + \zeta)/(\rho + P) \sim l_{\rm mfp}$. In addition to the sound mode, also long-lived, transverse shear modes can be excited in viscous fluid whose decay is governed by specific shear viscosity $\eta_s = \eta/(P+\rho)$. The explicit forms of the numerator structures $f_{\rm sound}(\omega, \vec{k})$ and $f_{\rm shear}(\omega, \vec{k})$ that are rational functions in $k_\perp$, k_z, and in ω are relegated to Appendix B.

The terms with viscosity are easily computed by completing the contour in the upper complex plane. As the hydrodynamic expression is valid up to linear order in η_s and Γ_s, we may expand the integrand to linear order in the viscosities. Then the only non-analytic features of the integrand arising from the sound channel on the upper complex half-plane are just given by the graviton pole $k^z_{grav} = -\frac{k_\perp}{\sqrt{v^2-1}}$ and another spurious pole given by $k^z_* = ik_\perp$. In the case $v < c_s$, there is an additional pole of the hydrodynamic propagator that is on the upper complex half plane $k^z_* = i\frac{c_s}{\sqrt{c_s^2 - v^2}}$ and the contribution simply reads

$$\begin{aligned}
{\rm Im}\int \frac{dk_z}{2\pi} k_z \left(\frac{1}{-(\omega+i\epsilon)^2 + \vec{k}^2}\right)^2 \frac{f_{\rm sound}(\omega,\vec{k})}{-\omega^2 + c_s^2 k^2 - ik^2\Gamma_s\omega} &= (P+\rho)\frac{\left(v^2+1\right)^2}{4v^2k_\perp^2}\theta(v-c_s) \qquad (32)\\
&+ (P+\rho)\frac{v\left(v^2+1\right)^2}{8c_s k_\perp \left(c_s^2 - v^2\right)^{3/2}}\theta(c_s - v)\Gamma_s \\
&+ \frac{(P+\rho)}{k_\perp v}\left\{\frac{(v^2-4)\sqrt{1-v^2} - 4v^2}{2} + \theta(c_s - v) 2\frac{c_s\left(v^2+1\right)}{\sqrt{c_s^2 - v^2}}\right\}\eta_s, \qquad (33)
\end{aligned}$$

where the first term corresponds to the ideal fluid dynamics and

$${\rm Im}\int \frac{dk_z}{2\pi} k_z \left(\frac{1}{-(\omega+i\epsilon)^2 + \vec{k}^2}\right)^2 \frac{f_{\rm shear}(\omega,\vec{k})}{\omega + i\eta_s k^2} = 2\frac{v(P+\rho)}{k_\perp}\eta_s \qquad (34)$$

We show the resulting drag force of the viscous fluid on the bullet and compare it to the ideal liquid behavior in Fig 2 where the red dashed lines correspond to the above expansion. As expected, the force does not vanish in the subsonic regime, where the viscous term is the proper leading order calculation of the force.

2. Breakdown of the gradient expansion at crossing the sound barrier

If the velocity of the projectile approaches the speed of sound from above, according to (30) the direction of the emitted phonons and the bullet coincide. In this case, the energy is not transmitted away from the projectile but the sonic boom created by the projectile follows its trajectory, see for example [10] for an illustration. Because the phonon travels with the bullet for an arbitrarily long time, it will become sensitive to viscous corrections for arbitrary small $k_\perp$. That this is the case

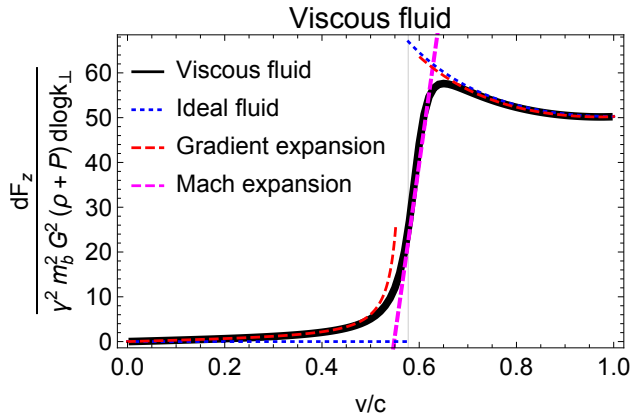

FIG. 2. The dynamical friction in realistic viscous fluids. For purposes of illustration we show the drag force for conformal fluid for which $c_s^2 = 1/3$ (marked by a vertical line) and $\zeta = 0$ and display the contribution arising from scale $k_\perp \Gamma_s = 0.01$. The thick black line corresponds to the drag force in viscous fluid computed directly from the correlation function of (31) without further expansions. This full result is compared to ideal hydrodynamics (blue dashed line, Eq. (29)), gradient expansion of the first-order fluid dynamics (red line, eqs. (32) (34)). The gradient expansion fails for velocities near the speed of sound $|v - c_s| < \frac{(\Gamma_s k_\perp)^{2/3}}{2c_s}$. Within this window, the ideal hydrodynamic expression receives $\mathcal{O}(1)$ viscous corrections irrespective of the magnitude of viscosities η and ζ. Within this window the drag is well described by the Mach expansion (purple dashed line, Eq. 38).

is seen explicitly in (32) where the relative correction to the ideal fluid result of (29) is enhanced near the Mach limit

$$F^z = F^z\Big|_{ideal\,fluid}\left[1 + \mathcal{O}\left(\frac{k_\perp \Gamma_s}{(c_s^2 - v^2)^{3/2}}\right)\right]. \tag{35}$$

This shows that for velocities in the window $|(v^2 - c_s^2)| < (k_\perp \Gamma_s)^{2/3}$ the first viscous corrections give a contribution comparable to the leading order correction and the leading order fluid-dynamical picture does not give correct description at any $k_\perp$ within this $k_\perp$-dependent window.

To clarify the source of this behavior, consider a bullet moving exactly at the speed of sound $v = c_s$. In this case, the leading order k^z-dependent part of the denominator sound propagator vanishes exactly and the unexpanded propagator reads

$$\frac{1}{-\omega^2 + c_s^2 k^2 - i k^2 \Gamma_s \omega} \xrightarrow{v=c_s} \frac{1}{c_s^2 k_\perp^2 - i c_s k^2 k^z \Gamma_s}. \tag{36}$$

The denominator is a cubic function of k^z and has three poles, one in the upper complex plane on the imaginary axis and two in the lower complex half-plane.[5] The location of the pole in the upper

[5] The two poles in the lower complex half-plane become the ideal hydrodynamic poles in the ideal limit at supersonic velocities. In the subsonic case, these two poles merge in the ideal limit to form the single pole in the lower complex half-plane of ideal fluid-dynamic propagator. The pole in the upper complex half plane reduces to the ideal one in the subsonic region and becomes irrelevant in the supersonic regime.

complex half-plane is inversely proportional to Γ_s and found straightforwardly by setting $k_\perp \ll k_z$ in (36)

$$k^z_{\Gamma_s} = i\frac{c_s^{1/3}(k_\perp \Gamma_s)^{2/3}}{\Gamma_s}, \tag{37}$$

see Fig. 4 for illustration. That is, upon approaching the Mach limit from below, the ideal-fluid-dynamic pole in the upper complex plane moves towards i-infinity, but the growth of the imaginary part is regulated by the viscosity and the pole goes far away from the real axis but remains in the finite complex plane. If we had expanded the denominator before taking the Mach limit, this pole would have not been present.

The contribution arising from this new pole—absent in ideal fluid dynamics—in the Mach limit is simply found by computing the integral on left hand side of equation (32), again completing the contour in the upper complex half-plane. The contribution arising from the pole of (37) gives

$$\begin{aligned}\mathrm{Res}\left[k_z\left(\frac{1}{-\omega^2+\vec{k}^2}\right)^2\frac{f_{\mathrm{sound}}(\omega,\vec{k})}{-\omega^2+c_s^2k^2-ik^2\Gamma_s\omega}, k^z_{\Gamma_s}\right] = \\ -(P+\rho)\frac{(1+c_s^2)^2}{6c_s^2k_\perp^2}\left[1-\frac{2}{3c_s^{1/3}}\frac{v-c_s}{(k_\perp\Gamma_s)^{2/3}}+\mathcal{O}(k_\perp\Gamma_s)+\mathcal{O}\left(\left(\frac{v-c_s}{(k_\perp\Gamma_s)^{2/3}}\right)^2\right)\right]\end{aligned} \tag{38}$$

It is noteworthy that in the first term, the factors of $1/\Gamma_s$ cancel exactly between the numerator and the denominator, such that the contribution is independent of Γ_s and remarkably survives even in the limit of ideal fluid $\Gamma_s \to 0$. That is, the fluid-dynamical expansion breaks down in the sense that first-order viscous corrections become as large as the leading order ideal fluid result near the Mach limit. However, the fluid-dynamical expansion still remains a good expansion in the sense that the corrections arising from second-order fluid dynamics—*i.e.* second order corrections to Eq. 20—still remain subleading compared to the full leading order result.

We finally note that the integral over k^z in (31) is straightforwardly performed analytically by computing the residues of the poles in the upper complex half-plane for any $v \neq c_s$ but leads to a complicated expression that we have decided not to include here (for a similar calculation in a different context, see [19]). Fig. 2 displays the drag force in conformal viscous fluid (with $c_s^2 = 1/3$ and $\zeta = 0$). The thick black line corresponds to evaluating Eq. 31 without making further expansions, whereas the red and purple dashed lines correspond to the gradient expansion of Eqs. (32) and (34) and the Mach expansion of (38), respectively.

B. Free streaming limit

We now discuss the drag force in the opposite limit of non-interacting medium. We provide results for a gas whose constituents may have any kinematics, thus extending the existing results on non-relativistic and ultra-relativistic approximations appearing in the literature.

In the absence of collisions, a system of freely streaming particles in a background metric $g^{\mu\nu}$ is described by transport equation

$$p^\mu \partial_\mu f(t,\vec{x};\vec{p}) - \Gamma^\alpha{}_{\beta\gamma} p^\beta p^\gamma \nabla^{(p)}_\alpha f(t,\vec{x};\vec{p}) = 0. \tag{39}$$

The distribution function f describes a distribution of on-shell particles whose energies are given by a dispersion relation $p^0 = E(\vec{p}) = \sqrt{|\vec{p}|^2 + m_g^2}$ and the partial p^0-derivative vanishes, $\nabla^{(p)}_0 f = 0$. Here m_g stands for the mass of the particles in the gas.

Assuming a small correction in the distribution function $\delta f = f - f_0$ due to the metric perturbation $h_{\alpha\beta}$, this equation is solved in Fourier space

$$\delta f = \frac{-i}{p^0} \frac{\Gamma^i{}_{\beta\gamma} p^\beta p^\gamma \nabla^{(p)}_i f_0}{-(\omega + i\epsilon) + \vec{v}_p \cdot \vec{k}}. \tag{40}$$

Here we have introduced the velocity $\vec{v}_p = \vec{p}/p^0$ of the medium constituent particles (not to be confused with the velocity of bullet in (7)). The numerator reflects the coupling of the medium constituent particles with the gravitational field and the denominator is the retarded eikonal propagator of the free-streaming particles; in coordinate space it reads $\sim \delta(\vec{x} - \vec{v}_p t)\theta(t)$. With this solution at hand it is simple to solve for the Green function of the energy-momentum tensor

$$G^{\mu\nu,\alpha\beta}_{kin} = \frac{\delta T^{\mu\nu}}{\delta h_{\alpha\beta}} \quad \text{with} \quad \delta T^{\mu\nu} = \int \frac{d^3p}{(2\pi)^3} \frac{p^\mu p^\nu}{p^0} \delta f \tag{41}$$

where the dependence on $h_{\alpha\beta}$ comes from the Christoffel symbols.

The dressed graviton propagator (11) can then simply be written with the aid of the solution δf (40), the definition of the energy-momentum Green function (41), and the graviton propagator (A3)

$$G^{dressed} = -i \int \frac{d^3p}{(2\pi)^3} \left(\frac{\kappa}{-(\omega+i\epsilon)^2 + k^2} \right)^2 I_{\gamma\delta,\mu\nu} I_{\alpha\beta,\rho\sigma} \frac{\delta \Gamma^i{}_{\omega\xi}}{\delta h_{\rho\sigma}} \frac{p_i p^\mu p^\nu p^\omega p^\xi}{(p^0)^2} \frac{f_0'(p^0)}{-(\omega+i\epsilon) + \vec{k}\cdot\vec{v}_p} u^\gamma u^\delta u^\alpha u^\beta \tag{42}$$

which we again study for $\omega = v k_z$. A similar result is found in, *e.g.*, [20]. Here we have also assumed that the unperturbed distribution function is isotropic, such that it only depends on the energies of particles p^0 and we may write $\nabla^{(p)}_i f_0 = \frac{p_i}{p^0} f_0'(p^0)$—anisotropic systems exhibit interesting dynamics that go beyond the scope of this work (see *e.g.* [21, 22] for complex dynamics in anisotropic non-Abelian plasmas). The projection tensors arising from graviton propagators

$I_{\gamma\delta,\mu\nu}$ are defined in the Appendix A. Expressing the integral over particle momenta in spherical coordinates $d^3p = p^2 dp d\Omega_p$ allows to perform the integral over the direction of the particles $d\Omega_p$

$$\mathrm{Im}\int k_z G^{dressed} dk_z = \mathrm{Im}\int k_z dk_z \int dp \frac{f'(p^0) p\gamma^4}{240\pi^2 (k_\perp^2 + k_z^2)^4 (p^0)^2 (k_\perp^2 - k_z^2(-1+v^2))^2} \times \left(R(k_z, k_\perp; p, p^0; v) + S(k_z, k_\perp; p, p^0; v) \log \frac{k_z p^0 v + \sqrt{k_z^2 + k_\perp^2}\, p}{k_z p^0 v - \sqrt{k_z^2 + k_\perp^2}\, p} \right) \tag{43}$$

where functions R and S arise from the numerator algebra in (42) and are fully analytic in all their variables—for the explicit form see Appendix B.

In order to perform the final integral over k_z it is again useful to consider the analytic structure of the integrand (42). Again, the integrand has non-analytic structures where propagators go on shell. As in the fluid-dynamic case, the graviton poles are located on the imaginary k_z-axis for $\omega = v k_z$. In contrast, the eikonal propagator of the in-medium particles $(-i\omega + i\vec{k}\cdot\vec{v}_p)^{-1}$ of (42) has poles on the the real axis for

$$|k_z/k| < v_p/v. \tag{44}$$

Upon integrating over the angles of the velocities of the particles $d\Omega_p$, the integral over the poles turns into the logarithm of (43) which has a branch cut along the real axis, see Fig. 4. The integration contour follows the real axis just above the cut to account for the $i\epsilon$ in (42)—to compute the imaginary part, it is enough to compute the discontinuity along the cut. Note that the function R is analytic and does not contribute to the drag force.

There are two distinct kinematic ranges that the integral over k_z can have depending on the momenta of the particles p. For particles whose velocity exceeds that of the bullet

$$p > \gamma m_g v, \tag{45}$$

the denominator of the logarithm is always negative, such that the branch cut extends over the entire real k_z-axis. The discontinuity of the branch cut of the logarithm is simply $2\pi i$, and the rest (the S functions and the prefactor) is simply integrated from minus to plus infinity. The final result reads

$$\begin{aligned}\mathrm{Im}\int k_z G_I^{dressed} dk_z = \frac{64\pi^2\gamma^4 G^2}{96\pi k_\perp^2 v^2} \int_{\gamma m_g v}^{\infty} dp\ \frac{p}{p^0}\frac{df_0}{dp^0} \times \\ \Big[2v\big(3p^4(-5+3v^2) + (p^0)^4(-27+29v^2) - 6p^2(p^0)^2(-7+9v^2)\big) + \\ 3(p^2-(p^0)^2)(-1+v^2)\Big((p^0)^2(9-5v^2) + p^2(-5+v^2)\Big)\log\left(\frac{1+v}{1-v}\right)\Big].\end{aligned} \tag{46}$$

Using $\frac{p}{p^0}\frac{df_0}{dp^0} = \frac{df_0}{dp}$ and performing the partial integral, the expression reads simply

$$\mathrm{Im}\int k_z G_I^{dressed} dk_z = -\frac{64\pi^2\gamma^4 G^2}{12\pi k_\perp^2 v^2}\int_{\gamma m_g v}^{\infty} dp\; p f_0 \times \Big[2m_g^2\left(v^2-3\right)v - 16p^2v^3 + 3m_g^2\left(v^2-1\right)^2 \log\left(\frac{1+v}{1-v}\right)\Big] \tag{47}$$

plus a boundary term at $p = \gamma m_g v$, which always exactly cancels with the $p < \gamma m_g v$ contribution as the integrand is continuous. Note that in the limit of ultra-relativistic medium the branch cut always extends over the entire real axis and therefore the entire contribution to the dynamical friction is given by (46) with the integration running from zero to infinity.

However, in the generic case this is not the only contribution. While the contribution to the integral from particles that move at velocities slower than the bullet

$$p < \gamma m_g v \tag{48}$$

is negligible in the case of ultra-relativistic particles, it becomes dominant in the non-relativistic limit. The branch cut is still located on the real axis, but it does not extend all the way to infinity. It is rather located between

$$-\frac{k_\perp p}{\sqrt{p^2(v^2-1)+v^2m_g^2}} < k_z < \frac{k_\perp p}{\sqrt{p^2(v^2-1)+v^2m_g^2}}. \tag{49}$$

The result of the integration in the second physical region is

$$\mathrm{Im}\int k_z G_{II}^{dressed} dk_z = \frac{64\pi^2\gamma^4 G^2}{48\pi k_\perp^2 v^2}\int_0^{\gamma m_g v} dp\; \frac{f_0'(p^0)p}{p^0} \times \Big[-3p(p^0)^3(9-14v^2+5v^4) + p^3p^0(29-54v^2+9v^4) + 3(p^2-(p^0)^2)(-1+v^2)\big((p^0)^2(9-5v^2)+p^2(-5+v^2)\big)\,\mathrm{arctanh}\left(\frac{p}{p^0}\right)\Big]. \tag{50}$$

Now let us compare the expressions that we have found to the known expressions in the literature, namely the ultra-relativistic and non-relativistic limits. The ultra-relativistic limit is simple to reproduce: as we have already mentioned, the branch cut extends over the entire real axis and only the dressed propagator from Eq. (46) contributes, with the lower integration limit trivially replaced by 0. In this limit the entire second term proportional to log inside the brackets vanishes, while the first term becomes

$$\frac{dF^z}{d\log k_\perp} = \frac{8m_b^2\gamma^2G^2}{3\pi}v\int_0^\infty \frac{p^5 f_0'(p)}{p}dp. \tag{51}$$

If one specifies the initial distribution to be the thermal distribution $f = e^{-p/T}$ for which the energy density is $\rho = 3T^4/\pi^2$, one obtains

$$F^z = \frac{64\pi}{3}G^2m_b^2\rho v\gamma^2\log\Lambda\ . \tag{52}$$

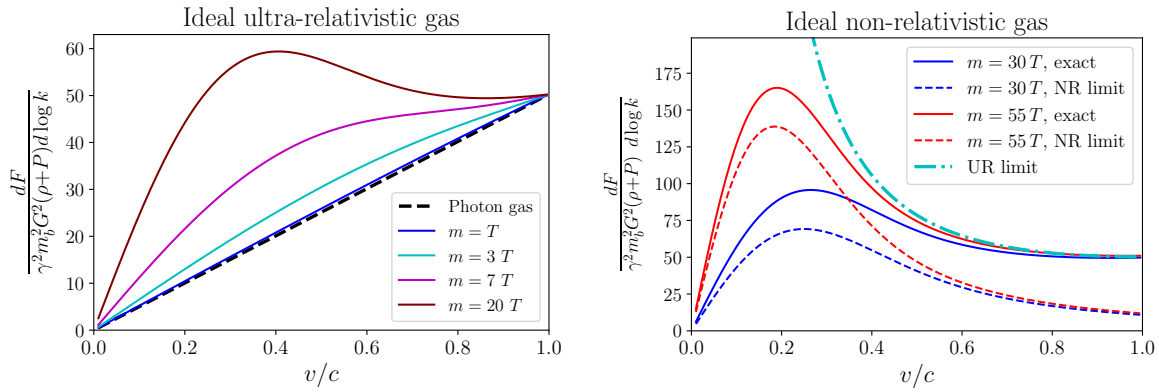

FIG. 3. The dynamical friction in ideal gas. The left panel shows the force in the regime of relativistic or nearly-relativistic gas, comparing the effect to the ultra-relativistic approximation. The right panel shows the drag force in largely non-relativistic gas. The solid lines show the exact result, while the dashed lines stand for the non-relativistic approximation of [1]. The dashed-dotted light blue line stands for the approximation of the relativistic projectile in a non-relativistic medium, Eq. (55).

Thus we readily recovered the result of [6], where $\Lambda \sim R_{\max}/R_{\min}$ arises from the regulation of the gravitational Coulomb divergence.

In the opposite limit, where both the bullet and the medium particles are moving at non-relativistic speeds ($v \ll 1$ and $v_p \ll 1$), we may expand the integrand in powers of p/m. We first notice that in this limit the dominant contribution to the integral over the momenta p comes from the region (50).

Expanding (50) to leading order in v and p/m and taking into account properly all the numerical factors in (16) one finds:

$$\frac{dF^z}{d\log k_\perp} = \frac{2}{3\pi}\frac{m_b^2 m_g^4 G^2}{v^2}\int_0^v f_0'(v')v'^3 dv' = \frac{2}{\pi}\frac{m_b^2 m_g^4 G^2}{v^2}\int_0^v f_0(v')v'^2 dv'. \tag{53}$$

Here we performed a change of integration variable $v' = p/m_g$ and at the last step integrated by parts. The would-be boundary term at $p = v$ again cancels exactly against a similar term in lower limit of the integral in (46).

The drag force is brought to the form of [1] by specifying the non-relativistic thermal distribution function $f_0 = e^{(\mu-m)/T}e^{-p^2/2mT}$, for which the energy density reads $\rho_{NR} = e^{(\mu-m)/T}\frac{m_g^{5/2}T^{3/2}}{(2\pi)^{3/2}}$. Performing the remaining integration gives the known result

$$F = \frac{(4\pi)^2 G^2 m_b^2 m_g}{v^2}\log\Lambda\int_0^v n(v')dv'\ , \tag{54}$$

where $n(v')$ is a number density of particles at given velocity v'.

We note that in addition to the above limits we can express the limit of a relativistic bullet propagating in non-relativistic gas in a simple form.

A priori, if the bullet is relativistic the contribution of the integral (46) is not suppressed by powers of the bullet velocity v and must also be taken into account. However, in the limit of the relativistic bullet and non-relativistic medium we expect $\gamma m_g v \gg T$ and therefore for a well-behaved distribution the contribution of (46) is exponentially suppressed. Therefore, in order to obtain this limit one should merely recover all the velocity factors in (50) and to carry the integration up to infinity, since this again will result only in exponentially suppressed corrections:

$$\frac{dF^z}{d\log k_\perp} = \frac{2}{\pi}\frac{m_b^2 m_g^4 G^2\gamma^2(1+v^2)^2}{v^2}\int_0^\infty f_0(v')v'^2 dv' = \frac{4\pi\rho m_b^2 G^2\gamma^2(1+v^2)^2}{v^2}\ , \tag{55}$$

where ρ is the energy density of the non-relativistic gas. We find in agreement with [10] that for a ultrarelativistic bullet, the form of the force is identical in both ideal gas and in ideal fluid.

Of course in the fully generic case, when we keep the mass of the medium constituent particles arbitrary, the result is more complicated and one may need to perform the integration over both contributions (46) and (50) numerically. It is instructive to compare the dynamical friction in the different kinematic ranges. In Fig. 3 we specify the thermal Maxwell distribution $f = e^{-p^0/T}$ and display the drag force for different m/T-ratios comparing to the non-relativistic and ultra-relativistic limits. For particles with masses $m \lesssim T$, the force is a monotonically rising function of velocity and is well described by the ultra-relativistic limit of (52) shown as the blue dashed line in the left panel of Fig. 3. As the mass is increased (or temperature decreased), the force as a function of v develops a characteristic shape of the non-relativistic limit (54), maximized when the velocity of the projectile is comparable to the medium particles $v \sim \langle v_p\rangle$ (red and blud dashed lines in the right panel). With finite m/T, the limit of large v coincides with the result in ideal gas (55) shown by the dash-dotted line in the right panel of Fig. 3.

C. Interacting kinetic theory

We now move on to compute the drag force in a full interacting kinetic theory model. The contributions to drag force arising from the two limits discussed in the previous sections—that is $k \gg 1/l_{\rm mfp}$ and $k \ll 1/l_{\rm mfp}$—are universal in the sense that they do not depend on the microscopic details of the interactions of the medium constituents. This is no longer the case for the contribution arising from the scale of the interactions $k \sim 1/l_{\rm mfp}$ which is sensitive to the specific form of the collision kernel. To study the qualitative features that are present in an interacting kinetic theory,

we will here concentrate in a particularly simple kinetic-theory model which retains qualitative features common to all interactions while still being analytically tractable. We study the kinetic theory in the *relaxation-time approximation* given by

$$p^\mu \partial_\mu f - \Gamma^\alpha{}_{\beta\gamma} p^\beta p^\gamma \nabla_\alpha^{(p)} f = \frac{p^\alpha u_\alpha^{\rm rest}}{\tau}(f - f_{eq}) \ , \tag{56}$$

where the collision kernel on the right hand side of the Boltzmann equation is based on the physical assumption that interactions bring the distribution function to its equilibrium form $f_{\rm eq}$ on a given relaxation timescale $\tau \sim \tau_{\rm scat} \sim l_{\rm mfp}/v_p$ in the local rest frame of the system $u_\alpha^{\rm rest}$ satisfying the Landau condition $u^\mu_{\rm rest} T^\nu_\mu = -\epsilon u^\nu_{\rm rest}$. While this model is a gross simplification of more realistic kinetic-theory models, it serves here as a prototype model to demonstrate the effect of finite interactions; in particular, it interpolates between free-streaming behavior at scales $k\tau \gg 1$ and ideal fluid behavior at scales $k\tau \ll 1$ [13]. The formalism here discussed can, of course, be applied to more complicated interactions as needed.

The retarded Green function of the energy-momentum tensor is known in the relaxation-time approximation in the massless limit. In order to study the drag force for systems with arbitrary masses and interaction rates, we extend these results for finite masses. Following closely the prescription of [13, 23] (see also [24]) and in close analogy to the free-streaming case, the perturbation of the distribution function δf caused by the gravitational perturbation $h_{\alpha\beta}$ has the formal solution

$$\delta f = -i \frac{\delta f_{eq}/\tau + \Gamma^\alpha{}_{\beta\gamma} \frac{p^\beta p^\gamma}{p^0} \nabla_\alpha^{(p)} f^g_{eq}}{-\omega + \vec{v}_p \cdot \vec{k} - i/\tau}, \tag{57}$$

which differs from the non-interaction result in two ways. The first difference is that the pole of the eikonal propagator moves in the negative complex plane by an amount i/τ reflecting the loss of correlation along particle trajectory because of interactions. The second difference arises because after the gravitational perturbation the local thermal equilibrium $f_{eq}(t,\vec{x}) = f^g_{eq} + \delta f_{\rm eq}(t,\vec{x})$ into which the interactions drive the system is not anymore same as the global thermal equilibrium f^g_{eq}. The local equilibrium $f_{\rm eq}(t,\vec{x})$ depends on the local value energy-momentum tensor $T^{\mu\nu}(t,\vec{x})$ that in turn depends on $\delta f_{eq}(t,\vec{x})$. The perturbation of the energy-momentum tensor $\delta T^{\mu\nu}$ needed for the Green function (41) can be obtained by first taking the appropriate integral moment of (57) to obtain a closed equation for $\delta T^{\mu\nu}$ that can be then self-consistently solved for $\delta T^{\mu\nu}$. The self-consistent solution generates additional poles which correspond to the fluid-dynamical poles for small $k\tau$, see Fig. 4.

Assuming a thermal Maxwell distribution $f^g_{eq} = e^{-p^0/\beta} = e^{u^{\rm rest}_\mu p^\mu/\beta}$, the perturbation of the

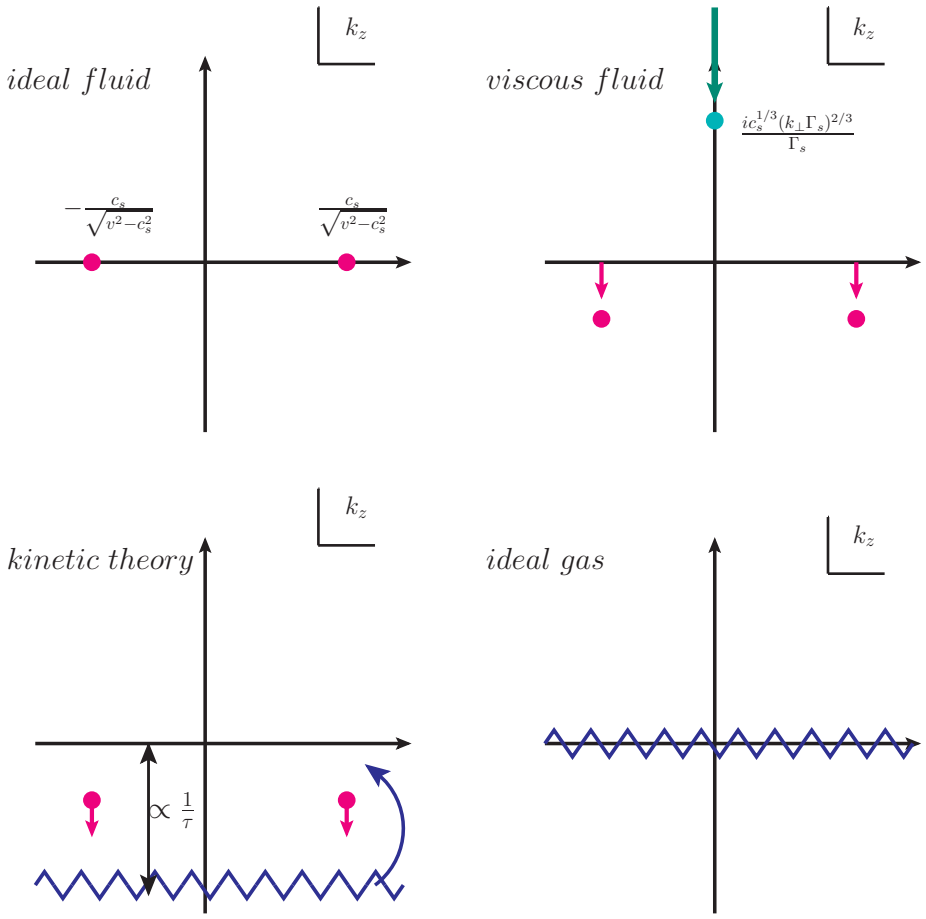

FIG. 4. The analytic structure of the retarded Green function of the energy-momentum tensor G^{medium} in fluid dynamics and in various regimes of the interacting kinetic theory. The ideal-fluid panel shows the poles when $v > c_s$. The arrows in the case of the viscous fluid show the motion of the poles in the complex plain as the sound attenuation length $\Gamma_s k^2$ is decreased. The arrows in the kinetic theory case show the motion of the poles and the quasiparticle cut as the scattering rate τ is decreased. When interpolating from fluid-dynamics to free streaming, the sound poles collide with the quasiparticle cut for $k\tau \approx 1$ and are hidden to the next Riemann sheet. In the free-streaming scenario ($\tau \to \infty$) only the quasiparticle cut remains.

local equilibrium distribution becomes

$$\delta f_{eq} = f^g_{\text{eq}}(p^0)\frac{p^0}{T}\left(\vec{v}_p \cdot \delta\vec{u}^{\text{rest}} + \frac{\delta T}{T}\right), \tag{58}$$

where $\delta\vec{u}$ is the perturbation of the local rest frame $u^{rest}(\tau, \vec{x})$ determined by the Landau condition. δT is the perturbation in the temperature $T(\tau, \vec{x})$ to which the interactions drive system locally,

given by the local energy density

$$\delta\rho = \delta T^{00} \qquad \text{with} \qquad \delta\rho = \frac{\partial\rho}{\partial T}\delta T \tag{59}$$

$$\delta u^i = \frac{\delta T^{0i}}{\rho + P} \qquad \text{with} \qquad \rho = \int \frac{d^3p}{(2\pi)^3} f_0(p) p^0(p). \tag{60}$$

Then taking the appropriate integral moment of (57) together with equations (59) and (60) gives a closed set of equations for $\delta T^{\mu\nu}$

$$\delta T^{\mu\nu} = \frac{-i}{T}\int \frac{d^3p}{(2\pi)^3}\frac{p^\mu p^\nu}{p^0}\frac{p^0\left(\vec{v}_p\cdot\vec{\delta u} + \frac{\delta T}{T}\right)/\tau - p^0\Gamma^i{}_{\beta\gamma}v^\beta v^\gamma v_i}{-\omega + \vec{v}_p\cdot\vec{k} - i/\tau} f^g_{\rm eq}(p^0), \tag{61}$$

The angular integral in this expression is simply performed similarly to the free-streaming case. The integral over the p is easily done in the massless case $m_g = 0$, but we have not found an analytic solution for arbitrary masses which we will solve numerically in the following.

Solving the above set of equations self-consistently with the definition (41) gives the full $G^{\rm medium}$ in the interacting kinetic theory. With this full solution at hand, we may simply read off the hydrodynamical coefficients that describe the fluid-dynamic properties of this kinetic theory model. In particular, the shear and bulk viscosities are extracted using Kubo relations

$$\eta = \lim_{\omega\to 0}\frac{1}{\omega}G^{xy,xy}(\omega, \vec{k} = 0) \tag{62}$$

$$\zeta = \frac{2}{9}\lim_{\omega\to 0}\frac{1}{\omega}G^{ii,jj}(\omega, \vec{k} = 0), \tag{63}$$

which—together with the speed of sound $c_s^2 = \frac{dP}{d\rho}$—fix the form of the correlation function in the large-wavelength limit. See Appendix D for the explicit integral expression of η and ζ. However, having the full correlation function at hand, we may go beyond the fluid-dynamic approximation.

After solving $G_{\rm medium}$, we can again proceed to compute to drag force by contracting the medium propagator with the the graviton propagators and integrating over $k_\perp$ and k_z, as per (16). Both ideal fluid and ideal gas are dissipationless, and both the sound modes in fluid and the free-streaming particles in gas are asymptotic states of the corresponding limits. This was reflected in that the non-analytic structures of $G_{\rm medium}$ were located on the real ω-axis in both cases. This is no longer the case at finite τ, where the finite interaction with the medium destroys any long-distance correlation and both the fluid-dynamic poles and the free-streaming cut move to negative complex half-plane of ω; the interplay between the hydrodynamical poles and the quasiparticle-cut is discussed in detail in [13, 23], see Fig. 4.

As the Green function of the energy-momentum tensor of the interacting kinetic theory is well approximated by ideal-fluid and ideal-gas limits at large and short distance scales, the contribution to the drag force arising from these scales also corresponds to the respective limits. This

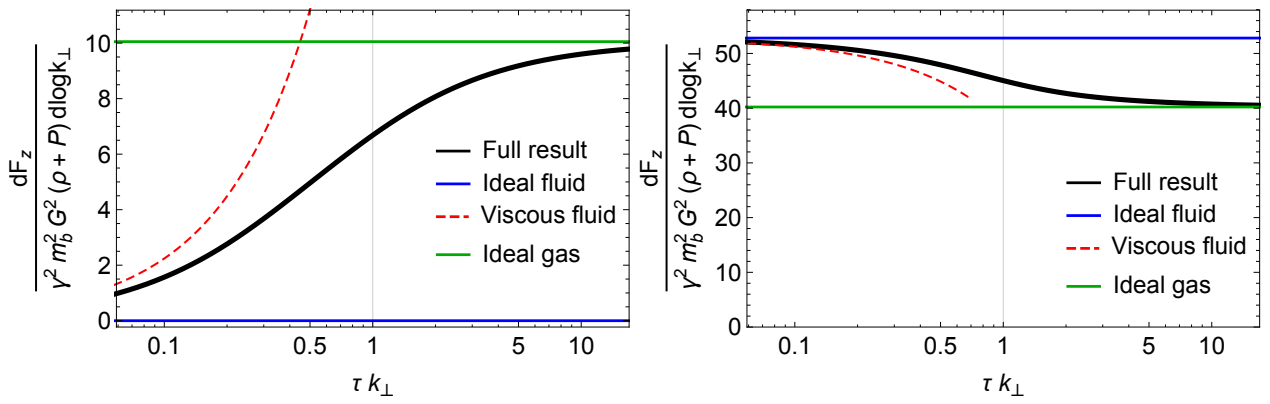

(a) $c_s > v = 0.2$. (b) $c_s < v = 0.8$.

FIG. 5. Differential drag force $dF^z/\log k_\perp$ as a function of $\tau k_\perp$ for a massless gas in interacting kinetic theory in relaxation-time approximation with $c_s^2 = 1/3$. At distance scales much shorter than the mean free path $k_\perp \tau \gg 1$, the full results asymptotes to the ideal-gas result (green line). At distance scales much longer than the mean free path $k_\perp \tau \ll 1$, the medium exhibits ideal-fluid behavior as demonstrated by the agreement of the full result (black line) with the ideal fluid-dynamic approximation (blue line). The approach to ideal fluid is described by the first-order viscous fluid dynamics shown by the red dashed line.

is demonstrated in Fig. 5, where we show the differential contribution to the force arising from different scales $\frac{dF^z}{d\log k_\perp}$. As expected, for small $k_\perp$ the full kinetic-theory contribution (black line) approaches the ideal-fluid result (blue line, Eq. (29)) and the first corrections in powers of $\tau k_\perp$ to the ideal-fluid result is captured by the viscous correction of (32) and (34). Note that for $v < c_s$, (left panel), the drag force vanishes in ideal fluid, but already the first viscous correction leads to finite correction. In the opposite limit of large $k_\perp$, the full result approaches the ideal gas value. For a subsonic projectile, the interacting kinetic theory approaches the ideal gas limit from below, while for a supersonic projectile the ordering is reversed.

In order to compute the total force, the differential force $\frac{dF^z}{d\log k_\perp}$ needs to be integrated over $\log k_\perp$ imposing a short- and a long-distance regulators to regulate the logarithmic Coulomb divergences. To provide the result in a way that does not depend on the regulators, we compute the difference between the full drag force and its leading-log expression

$$c_X = \int_{-\infty}^{\infty} d\log k_\perp \left[\frac{dF_z}{d\log k_\perp} - \theta(1-\tau k_\perp) \frac{dF_z}{d\log k_\perp}\bigg|_{\text{ideal fluid}} - \theta(\tau k_\perp - 1) \frac{dF_z}{d\log k_\perp}\bigg|_{\text{ideal gas}} \right], \quad (64)$$

where the expression form ideal fluid is given by (29) and for ideal gas in (47) and (50). This corresponds to the integral of difference between the full result and a step function switching from the ideal fluid to ideal gas at $\tau k_\perp = 1$ marked as a vertical line in Fig. 5. This expression is free of Coulomb divergences (for $v \neq c_s$) as the integrand vanishes by construction for large and

small $k_\perp$. We plot this quantity for medium of massless particles in Fig. 6 where we see that the subleading-log corrections are largest for $v \sim c_s$ where the correction diverges and changes sign.

The origin of this divergent behavior lies in the breaking of the fluid-dynamic gradient expansion near $v \approx c_s$ discussed in Section III A 2. The fact that near the Mach limit the drag force is never well described by ideal fluid dynamics is reflected in the fact that the remainder c_X obtains a large contribution down to $k_\perp \tau \sim (c_s^2 - v^2)^{1/3}$, (see Eq. (38)). To demonstrate this explicitly we also show the difference between the drag in viscous fluid compared to the ideal fluid for $k_\perp < 1/\tau$

$$c_X^{\rm visc} = \int_{-\infty}^{-\log\tau} d\log k_\perp \left[\left.\frac{dF_z}{d\log k_\perp}\right|_{\text{viscous fluid}} - \left.\frac{dF_z}{d\log k_\perp}\right|_{\text{ideal fluid}} \right]. \tag{65}$$

This is shown as the red dashed line in the left panel of Fig. 6. The divergent feature of c_X is contained in $c_X^{\rm visc}$ demonstrating that the breakdown of the leading-log expression arises from long-wavelength region where viscous fluid-dynamics still can be used even if the ideal hydrodynamic treatment fails. The remainder arising from the scale $1/\tau$, $c_X - c_X^{\rm visc}$, is indeed regular and numerically small at all v. The right panel of Fig. 6 shows $c_X^{\rm visc}$ for different masses of the medium constituent masses as function of Mach number v/c_s. We observe that by normalizing the contribution with $c_s^{3/2}$ motivated by Eq. (38), the different lines corresponding to different approximately collapse to single universal curve for $m \gg T$. The figure also displays displays the remainder $c_X - c_X^{\rm visc}$ for $m/T = 7$, which in analogy to the massless case is regular and numerically small.

Finally, Fig. 7 shows the full drag force in the interacting kinetic theory, for simplicity, in the massless limit. Because of the Coulomb divergence of the ideal-fluid and ideal-gas regimes the infrared and the ultraviolet regulators need to be implemented to arrive at a finite result. Here we implement a hard cut-off restricting the $k_\perp$ to an interval $1/R_{\rm max} < k_\perp < 1/R_{\rm min}$.

The left panel shows how system with finite mean free path interpolates between ideal-fluid-like and ideal-gas-like behavior as a function of the mean free path in a finite system with a constant external dimensions $R_{\rm max}/R_{\rm min} = 10^{12}$. The solid black line corresponds to a system that is ideal fluid at all scales, that is $\tau \ll R_{\rm min}$. The force in ideal fluid vanishes exactly in the subsonic regime and increases discontinuously at $v = c_s$. As the interaction rate is reduced the discontinuity is smoothened and the force is non-zero also for a subsonic projectile. We see that even if the mean free path is only slightly larger than the size of the projectile, say $\tau/R_{\rm min} = 10^2$ (green dashed line), there is substantial drag even in the subsonic regime. Eventually, as the mean free path gets larger and larger the ideal gas result is approached.

The right panel demonstrates how the dimensions of the system affect the drag force. In

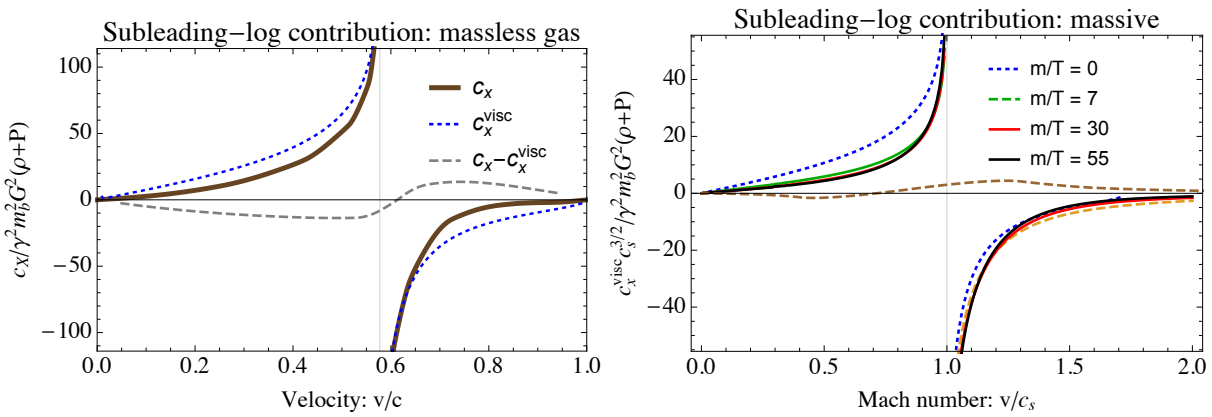

FIG. 6. The sub-leading-log contribution to the drag force. Left panel shows the contribution c_X computed in kinetic theory in relaxation-time approximation (thick brown line), and the corresponding quantity c_X^{visc} in first-order, viscous fluid dynamics (blue dotted line), as defined in Eq. (65). The gray dashed line corresponds to the difference to the two other lines, showing that the contribution arising from the l_{mfp}-scale is numerically small and regular. The right panel shows c_X^{visc} in non-confromal fluid dynamics corresponding to different m/T ratios. The dashed brown line shows $c_X - c_X^{visc}$ computed in the full interacting kinetic theory for $m/T = 7$ showing similar behavior as in massless case.

this figure, the mean free path is chosen to be within the external dimensions of the system, logarithmically equidistant from the cutoffs $R_{\rm max}/\tau = \tau/R_{\rm min}$, and the ratio $R_{\rm max}/R_{\rm min}$ is varied—for a meaningful comparison the force is normalized by the Coulomb logarithm $\log R_{\rm max}/R_{\rm min}$. In the limit of infinitely large system (black line, corresponding to the leading-log expression with $c_X = 0$) the discontinuity arising from ideal fluid dynamics is visible. As the system is made smaller with reducing $R_{\rm max}/R_{\rm min}$ the discontinuity rendered continuous by c_X. It is noteworthy that even in a system characterized by a large scale separation of $R_{\rm max}/R_{\rm min} = 10^{12}$ the discontinuity is markedly rounded.

IV. COMMENTS ON BOUNDARY EFFECTS

In the previous sections we assumed that the bullet has traveled in the medium for an infinite time and regulated the long-distance Coulomb divergence by considering a sharp IR-cutoff at $k_\perp = 1/R_{\rm max}$. If the bullet had traveled only a finite time in the medium, that would introduce a different IR regulator, and lead into different subleading-log contribution at the scale $R_{\rm max}$. Such a scenario was discussed in ideal fluid by Ostriker in [10], where it was found that also these effects render the drag a force a continuous function of velocity.

Without performing a full calculation, we discuss here how such finite boundaries can be included

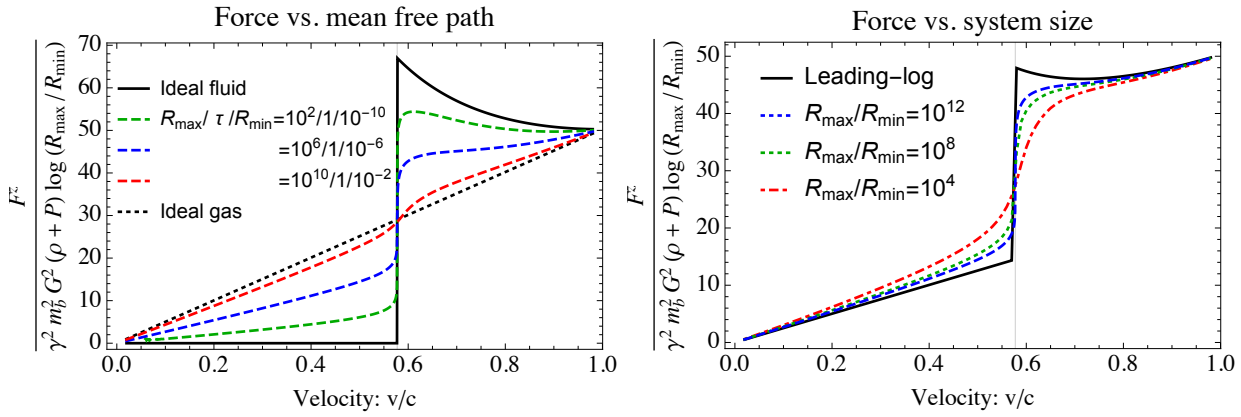

FIG. 7. The drag force in interacting kinetic theory. The left panel demonstrates the passage from a medium that is ideal fluid at all scales ($R_{\rm min} \ll \tau$, black solid line) to a medium that is ideal gas at all scales ($R_{\rm max} \ll \tau$, black dotted line). The other lines correspond the systems where the mean free path interpolates between the dimensions of the system $R_{\rm min} < \tau < R_{\rm max}$ keeping the external dimensions of the system fixed $R_{\rm max}/R_{\rm min} = 10^{12}$. The right panel demonstrates the effect of the external dimensions of the system. The different lines correspond to different UV- and IR-cutoffs: the black solid line corresponds to an infinite system, whereas the other lines correspond to finite systems with different $R_{\rm max}/R_{\rm min}$ ratios with a fixed $R_{\rm max}/\tau = \tau/R_{\rm min}$.

in our framework. The situation discussed in [10] is that of a medium that still has an infinite extent but the bullet appears in the unperturbed medium at time $t = 0$.

A similar setup can be manufactured in our framework by replacing the energy-momentum tensor of the bullet with a retarded one

$$T^{\mu\nu}_{bullet}(\vec{x},t) = \gamma\, m\, \delta(z - vt)\delta^2(\vec{x}_\perp)v^\mu v^\nu \times \theta(t), \tag{66}$$

$$\tilde{T}^{\mu\nu}_{bullet}(\vec{k},\omega) = \gamma\, m\, \frac{-iv^\mu v^\nu}{-\omega + k^z v - i\epsilon}. \tag{67}$$

Then the (derivative of) the gravitational field of the wake reads

$$\partial_\rho h^{wake}_{\mu\nu}(x_\perp = 0, z = vt > 0) = 64 i\pi^2 G^2 \gamma m v^\alpha v^\beta \int \frac{d^4k}{(2\pi)^4} e^{-it(\omega - ik^z v)} k_\rho G^{dressed}_{\mu\nu,\alpha\beta}(k) \frac{-iv^\mu v^\nu}{-\omega + k^z v - i\epsilon}, \tag{68}$$

and the force

$$F^z = \frac{m^2\gamma^2}{2} \int \frac{\mathrm{d}^2 k_\perp}{(2\pi)^2} \frac{\mathrm{d}k^z}{2\pi} k^z \frac{G^{dressed}}{-\omega + k^z v - i\epsilon} + m^2\gamma^2 \int \frac{\mathrm{d}^2 k_\perp}{(2\pi)^2} \frac{\mathrm{d}k^z}{2\pi} (\omega - k^z v) \frac{\tilde{G}^{dressed}}{-\omega + k^z v - i\epsilon} \tag{69}$$

with

$$\tilde{G}^{dressed} = G^{dressed}_{z\mu\alpha\beta} \tilde{v}^\mu v^\alpha v^\beta, \qquad \tilde{v}^\mu = \{1, 0, 0, -v\} \tag{70}$$

We leave further development and the evaluation of this expression for specific media to future studies.

V. DISCUSSION AND OUTLOOK

In this paper we have calculated the drag force in interacting relativistic medium.

Unlike in the previous works on this subject, we did not restrict ourselves to any particular kinematic regime, but presented a generic calculation that is valid at all masses and interaction rates. We showed that our techniques easily allow us to recover the previously known limits (relativistic and non-relativistic free-streaming gas, ideal fluid) as well as the interpolations between them. The results for viscous fluid, relativistic free-streaming gas and for interacting gas with a finite mean free path were presented for the first time. We studied interacting kinetic theory in a simple relaxation-time approximation and found that the important qualitative and quantitative features of the dynamical friction going beyond the leading-log approximation are reliably captured by the viscous fluid dynamics. Therefore, we believe that these features are unlikely to change if we consider other, more realistic models of particle interactions.

The calculation that we have presented here is merely the first attempt to tackle the dynamical friction problem with these new techniques. There are several obvious ways how one can improve these calculations, make them more precise, and even better suited for the practical problems in astrophysics. First, in this paper we have merely studied the Newtonian approximation. While it is sufficient for many practical problems, knowing the post-Newtonian corrections would be desired. While they have been considered in specific limits, a generic understanding of them in the case of generic masses and interaction rates is missing. One can, in fact, access the post-Newtonian corrections with our techniques by expanding to the next-to-leading order in the graviton loops, treating the gravity as an effective field theory [25]. Another useful application would be to understand the boundary effects on the dynamical friction appearing at scale $R_{\max}$. While we made the first step in Sec IV, there is still lots of room for progress, where one can consider the spatial-temporal boundaries [10] (invoking, *e.g.*, mirror charges). Also, more exotic media can be discussed (for recent work see, *e.g.* [14]). Finally, one can also study dynamical friction in non-linear movement, using the same formalism but changing appropriately the energy momentum tensor (for similar works using classical techniques see [26]).

Our results can be applied to a large number of astrophysical systems such as galactic dynamics with interacting dark matter (see *e.g.* [27]) and the interaction of primordial black holes with

neutron stars and white dwarfs. In particular, in setting limits on primordial black holes as a dark-matter component, the capture rate by compact objects is determined by dynamical friction in interacting and relativistic setting. Taking this into account, it will interesting to revise the previous bounds claimed by [2, 28]. The effects of dynamical friction in extreme conditions are also in an important role in studies of the hypothetical stable TeV-scale black holes [29]. With these new techniques and results here presented we expect to tackle these and many other questions.

Acknowledgments. We are grateful to Sergey Sibiryakov for numerous discussions and insights and collaboration at the early stages of this project as well as the comments on the manuscript. We are also grateful to Anton Rebhan for useful comments on the manuscript and Urs Wiedemann for useful discussions. A. Soloviev was supported by the Austrian Science Fund (FWF) doctoral program W1252.

Appendix A: Graviton propagator

For a generic linear perturbation of the energy momentum tensor $\delta T^{\mu\nu}$, the linearized Einstein equations in harmonic gauge ($\partial_\mu g^\mu{}_\nu - \frac{1}{2}\partial_\nu g^\mu_\mu = 0$) take the following form [25][6]

$$\Box\bar{h}_{\mu\nu} \equiv \Box(h_{\mu\nu} - \frac{1}{2}\eta_{\mu\nu}h) = \frac{1}{2}(\eta_{\mu\alpha}\eta_{\nu\beta} + \eta_{\mu\beta}\eta_{\nu\alpha} - \eta_{\alpha\beta}\eta_{\mu\nu})\Box h^{\alpha\beta} = 16\pi G\delta T_{\mu\nu}. \tag{A1}$$

We define a Green function for the above equation through,

$$\frac{1}{2}(\eta_{\mu\alpha}\eta_{\nu\beta} + \eta_{\mu\beta}\eta_{\nu\alpha} - \eta_{\alpha\beta}\eta_{\mu\nu})\Box G^{\alpha\beta,\gamma\delta}_{grav}(x,x') = 8\pi G(\eta^\gamma_\mu\eta^\delta_\nu + \eta^\delta_\mu\eta^\gamma_\nu)\delta^{(4)}(x-x') \tag{A2}$$

which is conveniently solved in Fourier space

$$G^{\mu\nu,\alpha\beta}_{grav}(x,x') = 8\pi G\frac{(\eta^{\mu\alpha}\eta^{\nu\beta} + \eta^{\mu\beta}\eta^{\nu\alpha} - \eta^{\alpha\beta}\eta^{\mu\nu})}{-(\omega+i\epsilon)^2 + k^2} \equiv 8\pi G\frac{I^{\mu\nu,\alpha\beta}}{-(\omega+i\epsilon)^2 + k^2}, \tag{A3}$$

such that

$$h_{\mu\nu}(x) = \int d^4x' G^{grav}_{\mu\nu,\alpha\beta}(x-x')T^{\alpha\beta}. \tag{A4}$$

[6] Note that our notation differs from that of [25] by $h_{here} = 8\pi G h$.

In addition [25] uses mostly minus metric such that $\Box_{here} = -\Box$.

Appendix B: Numerator structures

For completeness, we display here the full numerator structures appearing in Eq. 43

$$\begin{aligned}
R =& -2p\sqrt{k_\perp^2+k_z^2}\Big[2k_\perp^8(p^4(7v^4-10v^2+15)-15(p^0)^4(v^2+1)^2)\\
&+k_\perp^6k_z^2(8p^4(7v^4-10v^2+15)+15p^2(p^0)^2v^2(v^4+20v^2+16)+60(p^0)^4(v^6+7v^4-2))\\
&+k_\perp^4k_z^4\Big(12p^4(7v^4-10v^2+15)+5p^2(p^0)^2v^2(-33v^4+80v^2+144)\\
&-45(p^0)^4(v^8+16v^6-12v^4-8v^2+4)\Big)\\
&+4k_\perp^2k_z^6\Big(2p^4(7v^4-10v^2+15)-5p^2(p^0)^2v^2(5v^4+5v^2-36)\\
&+15(p^0)^4(6v^8-7v^6-5v^4+8v^2-2)\Big)\\
&+2k_z^8(p^4(7v^4-10v^2+15)+20p^2(p^0)^2v^2(2v^4-5v^2+6)-15(p^0)^4(2v^4-3v^2+1)^2)\Big]
\end{aligned}\tag{B1}$$

$$\begin{aligned}
S =& -15k_zp^0v\Big[k_\perp^8(p^4(v^4+2)+4p^2(p^0)^2(5v^2+1)+2(p^0)^4(v^2+1)^2)\\
&+2k_\perp^6k_z^2(p^4(v^4-2v^2+4)-p^2(p^0)^2(v^6+20v^4-22v^2-8)-2(p^0)^4(v^6+7v^4-2))\\
&+3k_\perp^4k_z^4(p^4(v^2-2)^2+2p^2(p^0)^2(3v^6-10v^4+2v^2+4)+(p^0)^4(v^8+16v^6-12v^4-8v^2+4))\\
&+4k_\perp^2k_z^6(v^2-1)(p^4(v^2-2)+p^2(p^0)^2(3v^4+3v^2-4)+(p^0)^4(-6v^6+v^4+6v^2-2))\\
&+2k_z^8(v^2-1)^2(p^2+(p^0)^2(1-2v^2))^2\Big]
\end{aligned}\tag{B2}$$

and

$$\begin{aligned}
f_{\rm sound}(\omega,\vec{k}) =& f_{\rm sound}^{\rm ideal}+\frac{\rho_0+P_0}{2}\Big\{4i\omega\Big[k^2\left(c_s^2\left(v^4+3\right)+2\left(v^2+1\right)\right)-2k_z^2v^2\left(c_s^2\left(v^2+3\right)+v^2+1\right)\\
&+\frac{4k_z^2v^3\left(c_s^2k_z^2v+\omega(2k_z+v\omega)\right)}{k^2}-\frac{4k_z^4v^4\omega^2}{k^4}-8k_zv\omega-\left(v^4+2v^2-3\right)\omega^2\Big]\eta_s\\
&+i\omega\left(v^2-3\right)\left[k^2\left(v^2+1\right)-\omega\left(8k_zv+\left(v^2-3\right)\omega\right)\right]\Gamma_s\Big\}
\end{aligned}\tag{B3}$$

$$f_{\rm shear}(\omega,\vec{k}) = -\frac{8(\rho_0+P_0)}{k^4}v^2\omega k_\perp^2\left(k^2+i\eta_s\left(2k^2k_zv-k_z^2v^2\omega\right)\right)\tag{B4}$$

Appendix C: Fluid-dynamic propagator

In this Appendix we consider the fluid dynamical response function studied extensively in literature (see *e.g.*, [12]). The starting point for the (1st order) relativistic dissipative fluid dynamics is the conservation of energy and momentum

$$\nabla_\alpha T^{\alpha\mu}=0,\tag{C1}$$

combined with a gradient expansion of the energy-momentum tensor including the terms containing at most one derivative of the flow and density fields $u^\mu(x)$ and $\rho(x)$. The most generic $T^{\mu\nu}$ is given

by the constitutive equation

$$T^{\mu\nu} = (\rho + P)u^\mu u^\nu + Pg^{\mu\nu} - 2\eta\sigma^{\mu\nu} - \zeta\nabla_\alpha u^\alpha \Delta^{\mu\nu},$$
$$\sigma^{\alpha\beta} = \frac{1}{2}\Delta^{\mu\alpha}\Delta^{\nu\beta}\Big(\nabla_\mu u_\nu + \nabla_\nu u_\mu - \frac{2}{3}\nabla_\alpha u^\alpha g_{\mu\nu}\Big) \equiv \langle \nabla^\alpha u^\beta \rangle, \tag{C2}$$

where η and ζ are the shear and bulk viscous transport coefficients, and where $\Delta^{\mu\nu} \equiv u^\mu u^\nu + g^{\mu\nu}$ is a spatial projector. We work in the Landau frame, *i.e.*, $u^\mu \sigma_{\mu\nu} = 0$.

In the following we will compute the linear response to a static and homogenous fluid with $\rho = \rho_0$ and $u_0^\mu = (1, 0, 0, 0)$ caused by a linear perturbation of the metric $g_{\mu\nu} = \eta_{\mu\nu} + h_{\mu\nu}$. The density perturbation is parameterized via $\rho = \rho_0 + \delta\rho(x)$ and the velocity perturbation as $u^\mu(x^\mu) = u^\mu + v^\mu(x^\mu)$, with $v^0 = 0$.

We now compute the linear response of the energy density and velocity induced by a plane-wave gravitational-field perturbation directed along the $\hat{l}$-direction

$$g^{\mu\nu}(x^\mu) = \eta^{\mu\nu} + h^{\mu\nu} e^{-i\omega t + i\vec{k}\cdot\hat{l}}. \tag{C3}$$

Inserting the constitutive equation C1 to energy conservation equation C1 and using the above ansatz, gives four equations that can be solved for the perturbations

$$\begin{aligned}
\delta\rho &= -\frac{1}{2}\frac{(\rho_0 + P_0)(k^2 h_{00} + 2\omega k h_{0l} + \omega^2 h_{ij}\delta^{ij}) + 2i\eta\omega k^2(h_{mm} + h_{nn})}{\omega^2 - c_s^2 k^2 + i\Gamma_s \omega k^2}, \\
v_m &= \frac{\eta\omega k h_{ml} + i(\rho_0 + P_0)\omega h_{0m}}{\eta k^2 - i\omega(\rho_0 + P_0)}, \\
v_n &= \frac{\eta\omega k h_{nl} + i(\rho_0 + P_0)\omega h_{0n}}{\eta k^2 - i\omega(\rho_0 + P_0)}, \\
v_l &= -\frac{1}{2}\frac{(c_s^2\omega k h_{ij}\delta^{ij} + \omega k h_{00} + 2\omega^2 h_{0l} - i\Gamma_s\omega^2 k h_{ij}\delta^{ij}) + 2i\eta\omega^2 k(h_{mm} + h_{nn})}{\omega^2 - c_s^2 k^2 + i\Gamma_s\omega k^2}
\end{aligned} \tag{C4}$$

where $\Gamma_s k^2$ is the sound attenuation length with $\Gamma_s = (\frac{4}{3}\eta + \zeta)/(\rho_0 + P_0)$.

Defining the fluid dynamical response function by[7]

$$\delta T^{\mu\nu}(x) = \int d^4x' G^{\mu\nu,\alpha\beta}_{medium}(x, x') h_{\alpha\beta}(x') \tag{C5}$$

$$\frac{\delta T^{\mu\nu}(\omega, \vec{k})}{\delta h_{\alpha\beta}} = G^{\mu\nu,\alpha\beta}_{medium}(\omega, \vec{k}) \times \begin{cases} 1, & \alpha = \beta \\ 1/2, & \alpha \neq \beta \end{cases} \tag{C6}$$

[7] Note that in the calculation we have chosen not to treat independently the off-diagonal elements of $h_{\mu\nu}$. However in the calculation of the force the two components get counted separately and for that reason we must divide the off-diagonal terms by a factor of two to avoid double counting.

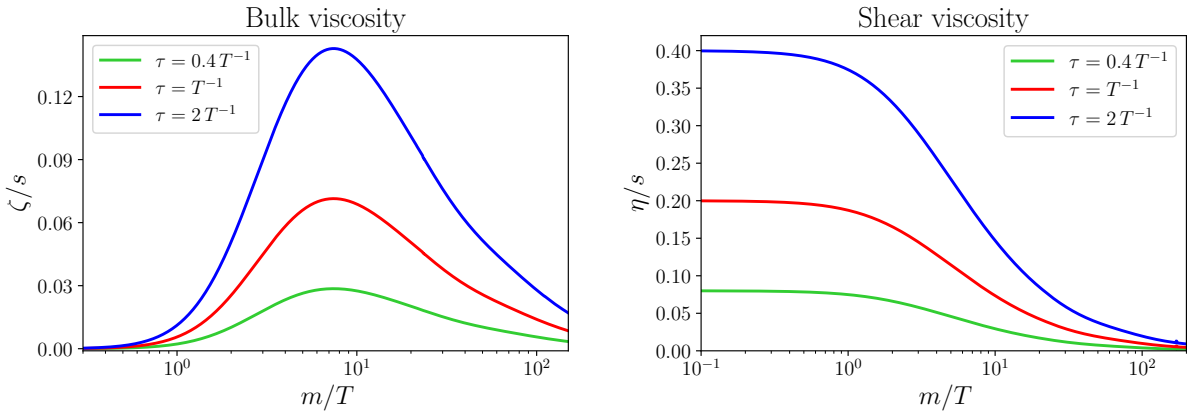

FIG. 8. Matching of the bulk viscosity onto the parameters of the full kinetic theory. The bulk viscosity, normalized to the entropy density is maximized around $m \sim 10T$. In the limit of zero mass of the gas particle both viscosities recover a well known conformal limit, $\zeta \to 0$ and $\eta \to sT\tau/5$.

one can straightforwardly find the components of the correlation function

$$G^{00,00}_{medium} = -\frac{(P_0+\rho_0)}{2}\frac{k^2}{-(\omega+i\Gamma_s k^2)^2+c_s^2k^2} - \rho_0 \tag{C7}$$

$$G^{0x,0x}_{medium} = -\frac{(P_0+\rho_0)}{2}\frac{i\eta\omega}{i\omega-\frac{\eta k^2}{\rho_0+P_0}} - \frac{P_0}{2} \tag{C8}$$

$$G^{xy,xy}_{medium} = \frac{i\eta\omega}{2} - \frac{P_0}{2} \tag{C9}$$

The first one corresponds to the sound channel, the second the shear channel and the last the tensor channel. The rest of the components can be obtained by the repeated use of the Ward identities, $\nabla_\mu T^{\mu\nu} = 0$, that relate components of the Green function within the different channels.

Appendix D: Extraction of Transport Coefficients from Kinetic Theory

In this appendix we match the the transport coefficient of the effective theory of viscous liquid onto the variable of full kinetic theory, namely the relaxation time τ and the mass of the gas particle m (for a very similar calculation see [30]). The result for the the Maxwell Boltzmann distribution reads

$$\eta = \int dp \frac{e^{-\frac{\sqrt{m^2+\vec{p}^2}}{T}} p^6 \tau}{30\pi^2(m^2+\vec{p}^2)} \tag{D1}$$

$$\zeta = \int \frac{dp e^{-\frac{\sqrt{p^2+m^2}}{T}} m p^4 \tau (p^2 K_2(m/T) - 3mTK_3(m/T)}{9(m^2+p^2)\pi^2(mK_2(m/T)+3TK_3(m/T)} \tag{D2}$$

where we have used to the specific heat

$$C_V = \frac{d\rho}{T d\log T} = \frac{m^3(\frac{m}{T}K_2(m/T) + 3K_3(m/T)}{2\pi^2} \tag{D3}$$

We plot both these transport coefficients on Fig. 8. Note that in the conformal limit we recover the well-known expression for $\eta/(\rho + P) \to \tau/5$, while the bulk viscosity vanishes.

---

[1] S. Chandrasekhar, *Dynamical Friction. I. General Considerations: the Coefficient of Dynamical Friction.*, ApJ **97** (Mar., 1943) 255.

[2] F. Capela, M. Pshirkov and P. Tinyakov, *Constraints on Primordial Black Holes as Dark Matter Candidates from Star Formation*, *Phys. Rev.* **D87** (2013) 023507, [1209.6021].

[3] F. Capela, M. Pshirkov and P. Tinyakov, *Constraints on primordial black holes as dark matter candidates from capture by neutron stars*, *Phys. Rev.* **D87** (2013) 123524, [1301.4984].

[4] P. Pani and A. Loeb, *Tidal capture of a primordial black hole by a neutron star: implications for constraints on dark matter*, *JCAP* **1406** (2014) 026, [1401.3025].

[5] F. Capela, M. Pshirkov and P. Tinyakov, *A comment on "Exclusion of the remaining mass window for primordial black holes ...", arXiv:1401.3025*, 1402.4671.

[6] D. Syer, *Relativistic Dynamical Friction in the Weak Scattering Limit*, MNRAS **270** (Sept., 1994) 205, [astro-ph/9404063].

[7] Y. Rephaeli and E. E. Salpeter, *Flow past a massive object and the gravitational drag*, ApJ **240** (Aug., 1980) 20–24.

[8] M. A. Ruderman and E. A. Spiegel, *Galactic Wakes*, ApJ **165** (Apr., 1971) 1.

[9] V. P. Dokuchaev, *Emission of Magnetoacoustic Waves in the Motion of Stars in Cosmic Space.*, Soviet Ast. **8** (Aug, 1964) 23.

[10] E. C. Ostriker, *Dynamical friction in a gaseous medium*, *Astrophys. J.* **513** (1999) 252, [astro-ph/9810324].

[11] E. Barausse, *Relativistic dynamical friction in a collisional fluid*, MNRAS **382** (Dec., 2007) 826–834, [0709.0211].

[12] R. Baier, P. Romatschke, D. T. Son, A. O. Starinets and M. A. Stephanov, *Relativistic viscous hydrodynamics, conformal invariance, and holography*, *JHEP* **04** (2008) 100, [0712.2451].

[13] P. Romatschke, *Retarded correlators in kinetic theory: branch cuts, poles and hydrodynamic onset transitions*, *Eur. Phys. J.* **C76** (2016) 352, [1512.02641].

[14] L. Berezhiani, B. Elder and J. Khoury, *Dynamical Friction in Superfluids*, 1905.09297.

[15] L. I. Petrich, S. L. Shapiro, R. F. Stark and S. A. Teukolsky, *Accretion onto a Moving Black Hole: A Fully Relativistic Treatment*, ApJ **336** (Jan., 1989) 313.

[16] E. P. Lee, *Dynamical Friction in the Post-Newtonian Approximation of General Relativity*, ApJ **155** (Feb., 1969) 687.

[17] S. A. Hartnoll and S. P. Kumar, *AdS black holes and thermal Yang-Mills correlators*, *JHEP* **12** (2005) 036, [hep-th/0508092].

[18] A. Kurkela, U. A. Wiedemann and B. Wu, *Flow in AA and pA as an interplay of fluid-like and non-fluid like excitations*, 1905.05139.

[19] R. B. Neufeld, B. Muller and J. Ruppert, *Sonic Mach Cones Induced by Fast Partons in a Perturbative Quark-Gluon Plasma*, *Phys. Rev.* **C78** (2008) 041901, [0802.2254].

[20] A. Rebhan, *Collective phenomena and instabilities of perturbative quantum gravity at nonzero temperature*, *Nucl. Phys.* **B351** (1991) 706–734.

[21] P. Romatschke and M. Strickland, *Collective modes of an anisotropic quark gluon plasma*, *Phys. Rev.* **D68** (2003) 036004, [hep-ph/0304092].

[22] A. Kurkela and G. D. Moore, *Thermalization in Weakly Coupled Nonabelian Plasmas*, *JHEP* **12** (2011) 044, [1107.5050].

[23] A. Kurkela and U. A. Wiedemann, *Analytic structure of nonhydrodynamic modes in kinetic theory*, 1712.04376.

[24] G. Baym, S. P. Patil and C. J. Pethick, *Damping of gravitational waves by matter*, *Phys. Rev.* **D96** (2017) 084033, [1707.05192].

[25] J. F. Donoghue, M. M. Ivanov and A. Shkerin, *EPFL Lectures on General Relativity as a Quantum Field Theory*, 1702.00319.

[26] H. Kim and W.-T. Kim, *Dynamical Friction of a Circular-Orbit Perturber in a Gaseous Medium*, *Astrophys. J.* **665** (2007) 432–444, [0705.0084].

[27] F. Kahlhoefer, K. Schmidt-Hoberg, J. Kummer and S. Sarkar, *On the interpretation of dark matter self-interactions in Abell 3827*, *Mon. Not. Roy. Astron. Soc.* **452** (2015) L54–L58, [1504.06576].

[28] P. W. Graham, S. Rajendran and J. Varela, *Dark Matter Triggers of Supernovae*, *Phys. Rev.* **D92** (2015) 063007, [1505.04444].

[29] S. B. Giddings and M. L. Mangano, *Astrophysical implications of hypothetical stable TeV-scale black holes*, *Phys. Rev.* **D78** (2008) 035009, [0806.3381].

[30] A. Czajka, S. Hauksson, C. Shen, S. Jeon and C. Gale, *Bulk viscosity of strongly interacting matter in the relaxation time approximation*, *Phys. Rev.* **C97** (2018) 044914, [1712.05905].